Dynamics on Six-Dimensional Potential Energy Surfaces for H 2 /Cu(111): Corrugation Reducing Procedure versus Modified Shepard Interpolation Method and PW91 versus RPBE

4 AUTHORS, INCLUDING:

Cristina Díaz
Universidad Autónoma de Madrid

55 PUBLICATIONS **804** CITATIONS

SEE PROFILE

Roar A. Olsen
SINTEF

60 PUBLICATIONS **2,116** CITATIONS

SEE PROFILE

Dynamics on Six-Dimensional Potential Energy Surfaces for H₂/Cu(111): Corrugation Reducing Procedure versus Modified Shepard Interpolation Method and PW91 versus RPBE

C. Díaz,*,†,§ R. A. Olsen,†,∥ H. F. Busnengo,‡ and G. J. Kroes†

Leiden Institute of Chemistry, Gorlaeus Laboratories, Leiden University, P.O. Box 9502, 2300 RA Leiden, The Netherlands, and Instituto de Física de Rosario (CONICET-Universidad Nacional de Rosario), Av. Pellegrini 250, 2000 Rosario, Argentina

We have constructed first principle based six-dimensional (6D) potential energy surfaces (PESs) describing the interaction of H₂ with Cu(111) obtained by interpolation of a set of density functional theory (DFT) total energy data. The DFT calculations have been performed within the generalized gradient approximation (GGA) framework. In applying the GGA we have tested the two exchange–correlation (XC) functionals most popular in surface science, i.e., the PW91 and RPBE functionals. The interpolation of the PW91 PES has been performed using two different methods, the corrugation reducing procedure (CRP), which has been proven to be one of the most successful interpolation methods to build 6D PESs, and the modified Shepard (MS) interpolation method, a very promising method to build high dimensional (*n*D) PESs, which is computationally cheaper than the CRP. We show that, in spite of the difference between the CRP-PES and the MS-PES and the inaccuracies found in the latter, quantum and classical reaction and scattering probabilities obtained for both PESs are very similar. We also show that PW91 predicts higher reactivity than RPBE, due to the presence of lower energy dissociation barriers in the PW91-PES. The differences between the PW91-PES and the RPBE-PES are also reflected in the vibrational excitation and rotational excitation probabilities, and the diffraction patterns.

Introduction

To generate a potential energy surface (PES) describing accurately the interaction between a molecule and a metallic surface has been a challenge for surface scientists studying molecule/surface dynamics for decades. Nowadays, for H₂ scattering from metal surfaces quantum dynamics methods can model motion in all molecular degrees of freedom (DOFs).[1−3] Therefore, the quality of theoretical results for diatomic molecules interacting with metal surfaces only depends on the quality of the underlying PES, provided that the approximations usually made (the Born–Oppenheimer and static surface approximations[1−3]) are reliable. A realistic dynamic simulation requires an accurate PES in many points along the region of configuration space accessible for the impinging molecules. To compute all the needed potential energy points by means of electronic structure calculations based on density functional theory (DFT) within the generalized gradient approximation (GGA) is very expensive from a computational point of view. A reasonable way to face this challenge is to use an interpolation method able to reproduce accurately the whole PES, by using a limited and reasonable number of DFT data.

The first molecule/surface dynamical studies made use of analytical PESs.[4−6] These analytical potentials, such as LEPS (London–Erying–Polanyi–Sato) PESs based on Morse potentials[7−9]

or methods based on symmetry adapted functions,[10,11] have been widely used. Although some sophisticated modified LEPS forms can describe complex molecule−surface PESs successfully,[12] the lack of flexibility of the standard LEPS has impelled the development of methods based on interpolation of DFT data. The methods based on interpolation of DFT data were first developed to build low-dimensional PESs.[13,14] But, now it is also possible to construct six-dimensional (6D) PESs based on DFT data thanks to the development of methods such as the corrugation reducing procedure (CRP)[15] and the modified Shepard (MS)[16] interpolation method (see below for detailed description of these methods). This latter method is a very promising method to build *n*D PESs with *n* ≥ 6, which would allow accurate dynamics studies of polyatomic molecules interacting with surfaces. Another interpolation method developed to model high dimensional PESs is based on neural networks,[17] which uses nonlinear fitting functions without any assumption about the functional form of the underlying problem. This method has already been used to perform a high-dimensional study of dissociation of H₂ on a (2 × 2) potassium-covered Pd(100) surface[17] and of dissociation of O₂ on a Al(111) surface.[18] Also a combination of the CRP with neural networks can be found in the literature.[19]

The CRP method is based on the interpolation of a DFT-GGA data set by combining analytical and numerical techniques.[15] The major advantage of this method is that the PES precision can be systematically improved by adding more data from DFT-GGA calculations. Its major disadvantage is that it cannot be extended straightforwardly to describe the interaction of polyatomic molecules with metallic surfaces. The CRP method has already been successfully used to build PESs for a

* To whom correspondence should be addressed. E-mail: cristina.diaz@uam.es.
† Leiden University.
‡ Instituto de Física de Rosario.
§ Current address: Departamento de Química Módulo 13, Universidad Autónoma de Madrid, 28049 Madrid, Spain.
∥ Current address: Akershus University College, P.O. Box 423, N-2001 Lillestrøm, Norway.

wide variety of molecule/surface systems, both nonactivated systems like H_2/Pd(111),[20,21] H_2/Ni(110),[22] H_2/Pd(110),[23] N_2/W(100),[24] H_2/Pt(211),[25] N_2/W(110),[26] H_2/W(100), H_2/W(110),[27] and H_2/Pd(100),[28] and activated systems like H_2/Ni(100), Ni(111),[22] H_2/Pt(111),[29] H_2/Cu(100),[29] H_2/NiAl(110),[30] H_2/Ru(0001),[31] H_2/Cu(110),[32] O_2/Ag(100),[33] H_2/Cu/Ru(0001), and H_2/Pd/Ru(0001).[34] Because the CRP method is very accurate, it can serve as a benchmark method for testing the accuracy of other, new interpolation methods.

The modified Shepard (MS) interpolation method,[35,36] which is based on a weighted series of second-order Taylor expansions, was developed to study gas phase reactions[37-41] and recently adapted for molecule/surface reactions.[16,42] It is a very promising method for polyatomic molecule/surface systems. For diatomic molecule/surface systems the MS method has an important advantage over the standard implementation of the CRP method: it potentially requires a smaller number of ab initio points, because the MS method focuses the interpolation on the dynamically important regions of the PES, whereas the CRP requires an homogeneous grid of ab initio points. The MS method has been used to describe the molecule−surface interaction in three activated systems, i.e., H_2/Pt(111),[16,42] N_2/Ru(0001),[43-45] and H_2/CO/Ru(0001),[46] and one nonactivated system, H_2/Pd(111).[47] In refs 16, 42, and 47, the MS PES was obtained by using a former CRP PES for the same system, in such a way that the CRP PES mimicked an ab initio code, giving, for any geometry, the value of the energy and the first derivatives, which were considered as the exact ones. In refs 44 and 45, the MS method was applied with a direct interface with a DFT code, but a comparison between the CRP and MS PESs where both were obtained directly from two independent DFT data sets has never been performed. This comparison is needed to judge the precision and performance of the modified Shepard method.

The reliability of the computed PES lays not only in the accuracy of the interpolation method but also in the accuracy of the GGA-DFT method itself. For gas phase reactions, systematic investigation with GGA functionals show that barriers calculated with these kind of functionals exhibit mean absolute errors higher than 0.2 eV.[48,49] These studies[48,50] show that for gas phase reactions higher accuracy can be achieved either from high-level ab initio theory or from hybrid DFT functionals. Unfortunately, both approaches are currently computationally too expensive to be used to map out a complete potential energy surface for a molecule−surface reaction. The use of hybrid functionals in DFT can be considered a promising method[51] to compute accurate PESs, but fundamental problems hinder a simultaneous accurate description of the molecule and the metal surface with this method.[52] Recently (see ref 53), it has been shown that it is possible to obtain accurate PESs describing molecule/surface systems by using the GGA-DFT method with a specific implementation of the SRP (specific reaction parameter) approach to DFT.[54]

Our aim with this study is 2-fold: (i) to determine whether the MS interpolation method directly interfaced with DFT yields accurate dynamics results for reaction and scattering, by comparison with dynamics results obtained with a CRP (accurately interpolated) PES, where the same exchange−correlation (XC) functional was used (PW91[55]); (ii) to study the dependence of the PES and dynamics results on the GGA-DFT XC functional used, where both PESs are based on DFT data interpolated with the CRP. To perform the latter analysis, in applying the generalized gradient approximation we have used the two most "popular" XC functionals in surface science, the

PW91[55] and the RPBE[56] (revised Perdew−Burke−Ernzerhof) functionals. The main difference between these two functionals is in the exchange part of the exchange−correlation energy, the RPBE exchange energy being more strongly dependent on the gradient of the electron density of the system than the PW91 exchange energy.[56] Thus, in total we have computed three PESs. We label these PESs as $y-x-$PES, where y is the interpolation method used, MS or CRP, and x is the functional used, PW91 or RPBE.

Methodology

Electronic Structure Calculations. To compute the PES data points, we assume that DFT with the use of the GGA for the exchange−correlation energy gives a semiquantitatively accurate description of a molecule−surface reaction if it proceeds adiabatically.[57,58] DFT equations are solved by using the DACAPO code,[59] which uses a plane wave basis set to describe the electronic orbitals and nonlocal ultrasoft pseudopotentials[60] for the ion cores. In applying the GGA we have used two functionals, PW91[55] and RPBE.[56] The DFT-PW91 energies have been obtained fully self-consistently,[53] whereas the DFT-RPBE ones have been estimated post-SCF using the electronic densities obtained in the fully self-consistent PW91 calculation. For a number of selected configurations, we have verified that the latter approximation is accurate enough for our purposes, e.g, the difference between the fully self-consistent RPBE and the nonself-consistent RPBE reaction barrier heights is less than 5 meV. The electronic minimization has been achieved by using the RMM-DIIS method and a Pulay density mixing scheme, within an absolute energy convergence of 10^{-5} eV. The computational parameters have been chosen to ensure that molecule/surface interaction energies, at important selected configurations such as the bridge-to-hollow barrier geometry, are converged to within about 0.05 eV.[53] This level of convergence, which is typical in PESs computed for molecules interacting with surfaces, was enough to ensure that the two GGAs (PW91 and RPBE) investigated here only reproduce molecular beam sticking experiments on D_2 + Cu(111) with semiquantitative accuracy. A four-layer Cu slab and a (2 × 2) surface unit cell have been used to model the adsorbate/substrate system, the distance between nearest neighbors for the Cu atoms in the top layer being $\Delta = a/\sqrt{2} = 2.62$ Å, where $a = 3.71$ Å is the bulk lattice constant obtained with the RPBE functional. This value is slightly larger than the value obtained for the PW91 functional, $a = 3.64$ Å, and than the experimental value, $a = 3.61$ Å. The interlayer distance has been relaxed (allowing all four Cu layers to move), having a final RBPE (PW91) value of 2.12 Å (2.11 Å), slightly expanded with respect to the experimental one of 2.08 Å for bulk Cu. The RPBE geometry of the relaxed slab has been used throughout the calculations of both the PW91 PES and the RPBE PES, as the differences between the RPBE and the PW91 values of Δ and of the relaxed interlayer distance were judged to be small enough to lead to only negligible changes in the molecule−surface interaction energy. A vacuum layer of 10.0 Å has been placed between the slabs in the Z direction to avoid artifacts caused by the use of periodic boundary conditions in the direction perpendicular to the slab. To sample the Brillouin zone, a 8 × 8 × 1 grid of Monkhorst−Pack special k-points has been used. For the plane-wave expansion a cutoff energy of 350 eV has been used, and 94 bands have been considered, as well as dipole corrections with a mixing parameter of 0.2. In all calculations the Cu atoms have been frozen to their equilibrium positions in the relaxed bare Cu slab. All the parameters we have used in the electronic

TABLE 1: DFT/PW91 Atomic Binding Reaction Energies, E^b_{H-Cu}, Atom−Surface Equilibrium Distances, z^b_{H-Cu}, and Reaction Energy (Including Zero Point Energy Corrections) for $^1/_2 H_2(g) \rightarrow H(ad)$, E^{rea}_{H-Cu} [a]

site	E^b_{H-Cu} (eV)	z^b_{H-C} (Å)	E^{rea}_{H-Cu} (eV/H-atom)
fcc	2.432 (2.271)	0.87 (0.90)	0.250 (0.051)
hcp	2.422 (2.261)	0.87 (0.91)	0.240 (0.041)
brg	2.287 (2.139)	1.03 (1.05)	0.105 (*b*)
top	1.796 (1.687)	1.53 (1.53)	*b* (*b*)

[a] Numbers in parentheses correspond to RPBE results. [b] The dissociative chemisorption over this site is endothermic.

structure calculations have been chosen on the basis of extensive convergence tests (see the Supporting Online Material for ref 53).

Using these parameters, we have found that the dissociation of H_2 on Cu(111) is an exothermic reaction with the maximum exothermicity obtained when the two atoms are bound at the fcc site (see Table 1), the energy released being 0.494 (0.102) eV/molecule for the PW91 (RPBE) functional, in good agreement with previous calculations.[32]

Finally, in selecting the configurations to be computed, we have assumed a C_{6v} symmetry for the fcc-Cu(111) surface although the point group symmetry for this surface is C_{3v}, which means that we consider fcc sites equivalent to hcp sites. In this case, we have only performed DFT calculations for the hcp hollow site. As discussed previously,[15,29] considering fcc and hcp hollow sites as equivalent ones is a reasonable approximation for the (111) metal surface due to the small energy differences between them.

Corrugation Reducing Procedure. In applying the CRP,[15,20] we take into account that the strongest variations of the 6D-PES come, mainly, from the repulsive interaction between the atoms of the molecule and the surface, when the molecule is close to it. After the atom/surface interactions is subtracted from the full PES, a smooth function remains (called interpolation function), which is much easier to interpolate than the corrugated full 6D-PES. Thus, the 6D-PES can be written as

$$V^{6D}(X,Y,Z,r,\theta,\varphi) = I^{6D}(X,Y,Z,r,\theta,\varphi) + \sum_{i=1}^{2} R_i^{3D}(X_i,Y_i,Z_i) \quad (1)$$

where the coordinates $(X, Y, Z, r, \theta, \varphi)$ represent the six degrees of freedom of the molecule over the surface (see Figure 1): the Cartesian coordinates of the molecular center of mass (X, Y), molecule−surface distance (Z), the distance between the atoms of the molecule (r), and the orientation of the molecule over the surface defined by the polar (θ) and azimuthal (φ) angles. $R_i^{3D}(X_i,Y_i,Z_i)$ represents the interaction energy of the ith atom of the molecule at (X_i, Y_i, Z_i) with the surface, and I^{6D} represents the 6D interpolation function. The interpolation of this smooth function is performed by using cubic spline interpolation over (Z, r), Fourier series over (X, Y), and trigonometric functions for (θ, φ); when the interpolation is performed over φ and θ, the molecular center of mass is kept fixed (see refs 21 and 29 for more details). To determine this interpolation function, the knowledge of the 3D-PES in all points of the 3D configuration space is required; thus another interpolation has to be applied. The 3D-PES is simpler than the 6D-PES, but still highly corrugated, which means that a direct interpolation of the DFT data cannot be used for the construction of $R_i^{3D}(X_i,Y_i,Z_i)$. Thus, to perform the interpolation of the 3D-PES, a strategy similar
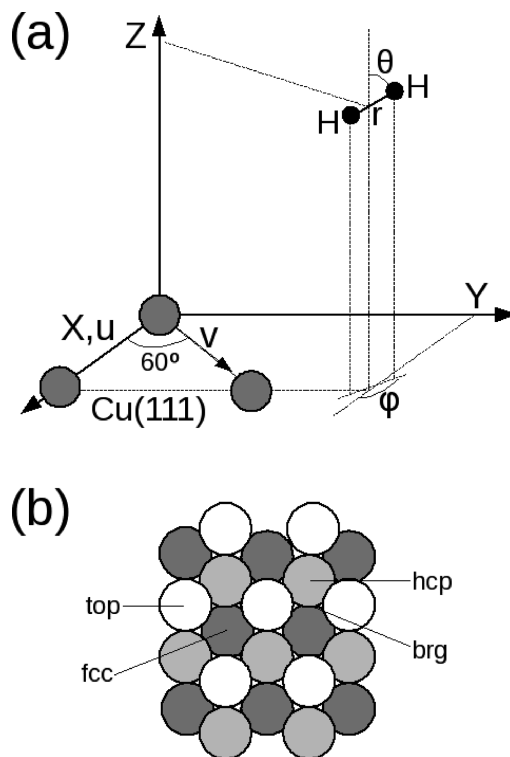

Figure 1. (a) Coordinate system used to define the position and orientation of H_2 relative to the Cu(111) surface. (b) High symmetry points of the Cu(111) surface. White spheres denote atoms in the first layer, light gray spheres denote atoms in the second layer, and dark gray spheres atoms in the third layer. Here (u, v) are defined by $u = X - Y/\sqrt{3}$ and $v = 2Y/\sqrt{3}$.

to the one used for the 6D-PES is applied. In this case, it is the repulsive interaction between an H atom and the surface atoms that causes the strongest variation of the 3D-PES. Therefore, similarly to the 6D-PES, the 3D-PES can be written as

$$R_i^{3D}(X_i,Y_i,Z_i) = J^{3D}(X_i,Y_i,Z_i) + \sum_{i=0}^{n} Q^{1D}(R_i) \quad (2)$$

where J^{3D} represents a 3D interpolation function and $Q^{1D}(R_i)$ is a 1D potential accounting for the short-distance repulsive interaction between the adsorbing atom and the ith atom of the surface.[15]

To compute the 3D interpolation function $R_i^{3D}(X_i,Y_i,Z_i)$, seven atomic impact sites have been used, each of them containing 53 points between −1.06 and +5.15 Å. These seven configurations are (i) $(X = 0, Y = 0)$, (ii) $(X = \Delta/6, Y = 0)$, (iii) $(X = \Delta/3, Y = 0)$, (iv) $(X = \Delta/2, Y = 0)$, (v) $(X = \Delta/2, Y = \Delta/2\sqrt{3})$, (vi) $(X = \Delta/4, Y = \Delta/4\sqrt{3})$, and (vii) $(X = 5\Delta/12, Y = \Delta/4\sqrt{3})$. The function $Q^{1D}(R)$ has been obtained by a spline interpolation of the DFT results for the top site. The interpolation function J^{3D} has been determined by performing a spline interpolation in Z for each site, and to interpolate this function in X and Y, a Fourier expansion has been used.

To parametrize the 6D-PES for H_2/Cu(111), we have carried out calculations for 18 two-dimensional (2D) cuts, defined by the molecular orientation (θ, φ) and the position (X, Y). For each 2D cut the molecule−surface distance Z has been varied from 0.25 to 4.0 Å and the H−H distance r from 0.4 to 2.3 Å. The configurations selected have been the following:

•Three configurations over the top site $(X = 0, Y = 0)$: (i) $\theta = 0$; (ii) $\theta = 90$, $\varphi = 0$; (iii) $\theta = 90$, $\varphi = 30$.

Potential Energy Surfaces for H₂/Cu(111)

J. Phys. Chem. C, Vol. 114, No. 25, 2010 **11195**

•Five configurations over the hollow site ($X = \Delta/2$, $Y = \Delta/2\sqrt{3}$): (i) $\theta = 0$; (ii) $\theta = 90$, $\varphi = 0$; (iii) $\theta = 90$, $\varphi = 30$; (iv) $\theta = 45$, $\varphi = 30$; (v) $\theta = 45$, $\varphi = 210$.

•Four configurations over the bridge site ($X = \Delta/2$, $Y = 0$): (i) $\theta = 0$; (ii) $\theta = 90$, $\varphi = 0$; (iii) $\theta = 90$, $\varphi = 60$; (iv) $\theta = 90$, $\varphi = 90$.

•Six configuration over the site halfway between the top and the hollow site ($X = \Delta/4$, $Y = \Delta/4\sqrt{3}$): (i) $\theta = 0$; (ii) $\theta = 90$, $\varphi = 30$; (iii) $\theta = 90$, $\varphi = 120$; (iv) $\theta = 45$, $\varphi = 30$; (v) $\theta = 45$, $\varphi = 120$; (vi) $\theta = 45$, $\varphi = 210$.

In total we have computed 3899 DFT points, 3528 for H₂/Cu(111) and 371 for H/Cu(111).

Modified Shepard Interpolation Method. In the modified Shepard interpolation method[35,61] the 6D-PES is given by a weighted series of second-order Taylor expansions centered on DFT data points, sampled throughout the configuration space. Thus, the total potential energy at any configuration ζ is given by

$$V(\zeta) = \sum_{i=1}^{N_{\text{data}}} w_i(\zeta)\, T_i(\zeta) \qquad (3)$$

where N_{data} is the number of DFT data used in the interpolation, the term $w_i(\zeta)$ represents a normalized weight function,[36] and $T_i(\zeta)$ represents the second-order Taylor expansion of the potential centered on the data point $\zeta(i)$,

$$T_i(\zeta) = V[\zeta(i)] + \sum_{k=1}^{3n-6} [\zeta_k - \zeta_k(i)]\frac{\partial V}{\partial \zeta_k}\bigg|_{\zeta(i)} + \frac{1}{2}\sum_{k=1}^{3n-6}\sum_{j=1}^{3n-6}[\zeta_k - \zeta_k(i)][\zeta_j - \zeta_j(i)]\frac{\partial^2 V}{\partial \zeta_k \partial \zeta_j}\bigg|_{\zeta(i)} \qquad (4)$$

where the coordinates (ζ_i) of the vector ζ are defined as linear combinations of the inverse interatomic distances between the n atoms of the system; in our case $n = 5$ because we only need the 2 atoms of H₂ and 3 atoms of Cu to model the system.[45] To evaluate the Taylor expansions, the energies and gradients are computed analytically by using the DACAPO code. The second derivatives are calculated numerically from the gradients using forward differencing.

The advantage of the MS method over the CRP is the use of a nonuniform sampling of DFT data points, which allows us to focus on the so-called dynamically important regions, which are selected by means of classical dynamics. To choose the DFT points, an iterative scheme is used. Schematically:

(i) We build a initial PES, which only includes 64 points located along 4 reaction paths corresponding to high symmetry sites, including the bridge to hollow reaction path, where the minimum reaction barrier is located, the top to bridge and the top to hollow reaction paths, and a reaction path for which the molecular center of mass is located over the hcp site.

(ii) Using this initial PES, we run 10 classical trajectories, and along each trajectory we store periodically the molecular geometries explored by the molecule.

(iii) From the stored geometries we choose and add a new point to the PES, based on two different criteria:[35,36] (1) The "h-weight" criterion locates data points in the regions most frequently visited by the classical trajectories. (2) The "variance" criterion locates new points in regions where the interpolated energy is suspected to be the most inaccurate. It is based on
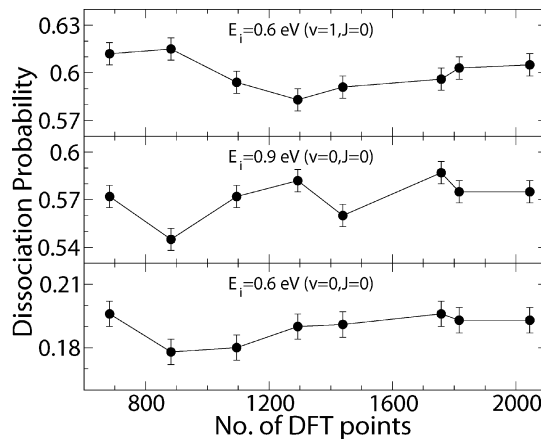

Figure 2. Dissociation probability as a function of the number of DFT points added to the PES data set, for two different incidence energies and two rovibrational initial states.

TABLE 2: Kinetic Energies and Rovibrational States (v, J) for Which the PES Data Set Has Been Grown

(v, j)	energies (eV)
(0, 0)	0.5, 0.7, 0.9, 1.1
(0, 1)	0.5, 0.7, 0.9, 1.1
(0, 2)	0.5, 0.7, 0.9, 1.1
(0, 6)	0.5, 0.7, 0.9, 1.1
(0, 11)	0.5, 0.6, 0.7, 0.8, 0.9
(1, 0)	0.4, 0.6, 0.8, 1.0
(1, 1)	0.4, 0.6, 0.8, 1.0
(1, 2)	0.4, 0.6, 0.8, 1.0
(1, 6)	0.3, 0.4, 0.5, 0.6, 0.8

the assumption that the accuracy of the PES will be best improved if new points are added in these inaccurate regions.

(iv) Once the PES is updated, the growth process is restarted at step ii.

(v) The growth of the PES is stopped when the dissociation probability is considered to be converged to within a given tolerance (0.005 in this case). The convergence is checked approximately every 200 added points, by performing more extensive classical trajectory simulations ($\approx$5000 trajectories).

Our PES has been converged after adding a total of 2000 data points. The convergence process is shown in Figure 2, where we show the dissociation probability as a function of the number of data points present in the PES data set, for several initial energies and rovibrational states. To ensure the accuracy of the PES over a wide range of energies, we have grown the PES using simultaneously several translational energies and initial rovibrational states (see Table 2).

Classical and Quantum Dynamics. The 6D Hamiltonian describing the motion of a diatomic molecule relative to the skewed surface unit cell of Cu(111) can be written as (in atomic units):[62]

$$\hat{H} = -\frac{1}{2M}\frac{\partial^2}{\partial Z^2} - \frac{2}{3M}\left(\frac{\partial^2}{\partial u^2} - \frac{\partial}{\partial u}\frac{\partial}{\partial v} + \frac{\partial^2}{\partial v^2}\right) - \frac{1}{2\mu}\frac{\partial}{\partial r^2} + \frac{\hat{j}^2}{2\mu r^2} + V_{6D}(u,v,Z,r,\theta,\varphi) \qquad (5)$$

Here, M and μ are the total and the reduced mass of the molecule, respectively, $\hat{j}$ is the angular momentum operator describing the molecule's rotation, and V_{6D} represents the 6D potential describing the interaction of the H₂ molecule with the Cu surface.

On the basis of the above Hamiltonian, we have performed both quasi-classical (QC)[63] and quantum (Q) dynamics[2] simulations. To compute QC dissociation probabilities, the Hamilton (or Newton) equations of motion have been solved by using the predictor-corrector method of Bulirsch and Stoer[64] (or the velocity-Verlet algorithm[65]). At the end of the trajectory we consider that dissociation has taken place whenever the interatomic distance reaches 2.25 Å with a positive radial velocity. The QC dissociation probabilities are given as an average over the molecular initial internal coordinates and internal conjugated momenta, obtained by using a conventional Monte Carlo method. To ensure low statistical errors (typically smaller than 5%, with absolute errors between 0.001 and 0.0035), 20 000 trajectories have been computed for each initial set of translational and rovibrational energies. The choice of QC over pure classical (C) calculations has been based on previous studies showing that QC simulations describe activated systems better than C ones.[2,3,66−68] This is thanks to the inclusion of the zero point energy of the molecule in the QC calculations, which allows taking into account vibrational softening, i.e., the adiabatic transfer of energy from internal to translation motion, which accelerates the molecule when approaching the surface, increasing the dissociation probability.[21]

Quantum dynamics calculations have been carried out using a time-dependent wave packet method.[69] In the implementation used,[70] the wave packet is propagated according to the time-dependent Shrödinger equation using the split operator method.[71] A Fourier representation (DVR, discrete variable representation.)[72] is used to represent the dependence of the wave function on u, A v, Z, and r, and fast Fourier transforms[73] to transform the wave function from the coordinate representation to the momentum representation, and vice versa. An indirect product FBR (finite basis representation) is used for the rotations, employing Gauss−Legendre and Fourier transformations to switch between the DVR and FBR.[74] The initial wave function is the product of a Gaussian wave packet in Z, a plane wave function for the motion parallel to the surface and a rovibrational wave function describing the initial state of H_2. The reflected wave packet is analyzed by computing **S**-matrix elements using a formalism developed by Balint-Kurti et al.[75,76] The reaction probabilities are obtained by summing the scattering probabilities and subtracting the result from unity. The relevant computational parameters to the wave packet calculations are listed in Table 3.

Results

Accuracy and Details of the PESs. To test the accuracy of the interpolated CRP-PW91-PES and MS-PW91-PES we have compared interpolated data with DFT data not used in the interpolation process. We have mainly focused on the entrance channel because, as we discuss below, this is the most important region for the dynamics. In Figure 3a−d we show the θ dependence of the CRP-PW91-PES and the MS-PW91-PES for configurations with the center of the molecule over the bridge site (Figure 3a), over two sites along the top-bridge line (Figure 3b,c), and over a low symmetry site (Figure 3d). In Figure 3e,f we show the φ dependence for several low symmetry configurations, and in Figure 3g,h we show the ρ dependence ($\rho = (X^2 + Y^2)^{1/2}$, X and Y being the coordinates that represent the displacement parallel to the surface) for the center of the molecule moving along the top-bridge line (Figure 3g) and moving along the top-hollow-bridge line (Figure 3h). From these figures we can see that the agreement between the DFT data and the interpolated CPR-PW91-PES is excellent. In particular, the CPR-PW91-PES reproduces very well the change of the energetically most favorable orientation from perpendicular to parallel when a molecule approaches the surface, as shown by the DFT data (Figure 3a). These tests show interpolation errors not larger than 0.03 eV. Although the comparison we have shown above corresponds to the PES obtained using the PW91 functional, similar results have been obtained for the CRP-RPBE-PES.

The agreement between DFT data and the MS-PW91-PES is very good for intermediate molecule−surface distances, especially for high symmetry configurations. When the molecule is close to the surface, the agreement worsens, becoming even poor for some configurations, which is consistent with the fact that few points used in the MS interpolation are located in the region close to the surface, which is not important to the dynamics. As shown in Figure 4a, where we have plotted the location of the computed DFT points projected on the (Z, r) plane, most of the DFT added points are located in the entrance channel (low r and high Z values). This reflects the fact that the most important dynamical region for H_2/Cu(111) is the one corresponding to the valley of the reactants; i.e., the probability of a molecule to be dissociated (or reflected) depends on the trajectory followed by the molecule until it reaches the reaction barrier or is reflected from it. From these results, we expect reaction and scattering probabilities to be accurate, in spite of the fact that for molecular configurations close to the surface the MS method does not give good results. We also show in Figure 4b the distribution of the added points over the (X, Y) plane (over the irreducible wedge of the surface unit cell). From this figure we can see that the distribution is rather uniform.

In Figure 5 we show several 2D contour plots in (Z, r) comparing the CRP-PW91-PES, the MS-PW91-PES, and the CRP-RPBE-PES. This allows us to evaluate how the PES characteristics are affected by the choice of the interpolation method and the exchange−correlation functional. From this figure we see first that the 2D plots corresponding to the MS-PW91-PES (Figure 5A−C) are rather *bumpy*, due to the use of a nonhomogeneous grid of DFT points. However, the main characteristic of the PES that determines the reactivity of the system, i.e., the positions and heights of the reaction barriers, and the curvature of the elbows are in reasonably good agreement with those obtained from the CRP-PW91-PES (Figure 5D−F). For this reason we expect similar dynamical results using either PES. For example, the minimum reaction barrier height in the MS-PW91-PES is 0.51 eV, located on the
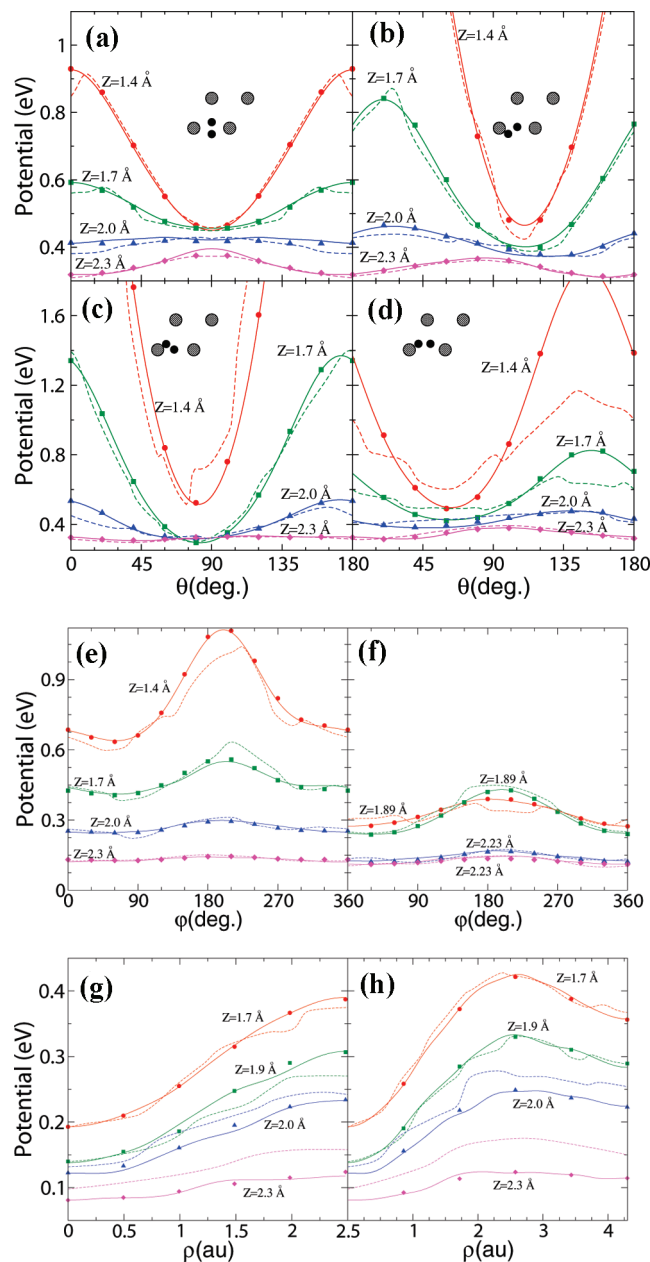
Potential Energy Surfaces for H₂/Cu(111)

J. Phys. Chem. C, Vol. 114, No. 25, 2010 **11197**

Figure 3. Comparison of the H₂/Cu(111) CRP-PW91-PES (solid line) and the MS-PW91-PES (dashed line) with DFT results (symbols) not used in the input data set. The four top panels represent the θ dependence for four configurations, for several Z values, centered on (a) $u = \Delta/2$, $v = 0$, $\varphi = 90$ $r = 0.9$ Å; (b) $u = \Delta/6$, $v = 0$, $\varphi = 30$ $r = 0.9$ Å; (c) $u = \Delta/3$, $v = 0$, $\varphi = 135$ $r = 0.9$ Å; and (d) $u = \Delta/3$, $v = \Delta/6$, $\varphi = 0$ $r = 0.9$ Å. The two middle panels represent the φ dependence for several random configurations centered on (e) $u = \Delta/3$, $v = \Delta/6$, $\theta = 135$ $r = 0.75$ Å; and (f) in red $\theta = 90$, $r = 0.81$ Å, $u = 0.075\Delta$, $v = 0.02\Delta$, in green $\theta = 90$, $r = 0.81$ Å, $u = 0.2\Delta$, $v = 0.1\Delta$, in blue $\theta = 90$, $r = 0.78$ Å, $u = 0.2\Delta$, $v = 0.1\Delta$, and in magenta $\theta = 90$, $r = 0.78$ Å, $u = 0.075\Delta$, $v = 0.02\Delta$. The two bottom panels represent the ρ dependence (see text) for (g) $\theta = 90$, $\varphi = 45$ $r = 0.8$ Å along the top-bridge line; and (h) $\theta = 135$, $\varphi = 45$ $r = 0.8$ Å along the top-hollow-bridge line.

bridge site, just slightly higher than the value of 0.49 eV found for the CRP-PW91-PES (Figure 5A,D). In the case of the RPBE-CRP-PES (Figure 5G–I) the minimum reaction barrier is also located at the bridge-to-hollow geometry (Figure 5G), but it is 0.33 eV higher ($E_B = 0.82$ eV). A similar behavior of the RPBE-PES with respect to the PW91-PES, i.e., the presence of higher reaction barriers, has been found previously, for example, for
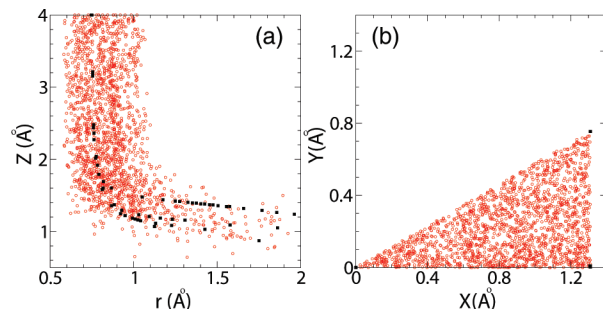

Figure 4. MS-PES data set projected on (Z, r) (a) and on (X, Y) (b) (black squares) initial DFT points; (red circles) added DFT points.

H₂/Ru(0001),[31] N₂/Ru(0001),[44] and N₂/W(100) and N₂/W(100).[78] Although the results for the minimum reaction path seem to indicate that the difference between the PW91-PES and the RPBE-PES is mostly a rigid shift in energy between them, the other two configurations displayed in Figure 5E–F and Figure 5H–I also show some differences in the location of the reaction barriers.

In Figure 6, we show PW91 and RPBE potential energy curves (Figure 6A) and the difference between them (Figure 6B) as a function of Z, for several configurations, all of them with $r = r_{eq}$ (r_{eq} being the H–H equilibrium distance in vacuum). The differences between the PW91 and the RPBE energies increase when the molecule–surface distance decreases (see Figure 6B). A quick look at Figure 6A could suggest that RPBE energies are systematically larger than the corresponding PW91 ones. But a more detailed analysis (see Figure 6B) reveals differences in the shape of the corresponding potentials. For example, two of the configurations represented in Figure 6, over the bridge site, show PW91 energies lower than the RPBE ones far and close to the surface, but higher PW91 energies for intermediate distances. Thus the CRP-RPBE-PES is not just a rigid energy shift of the CRP-PW91-PES. The same conclusion was reached previously for H₂/Ru(0001).[79]

We have also studied the energetic and the geometric corrugation for the three calculated PESs. The energetic corrugation is defined as the difference between the lowest barrier height found at the site displaying the lowest overall barrier height (bridge site) and the lowest barrier height found at the site displaying the highest overall maximum barrier height (hcp site), for the molecule oriented parallel to the surface. The geometric corrugation is defined as the difference between the positions of the earliest (top site) and latest (bridge site) barrier. We have found that both the energetic and the geometric corrugations are very similar for the three PESs (see Table 4).

Dynamics Results. To check the ability of the MS PES to give accurate dynamics results, we have computed several observables using both the MS-PW91-PES and the CRP-PW91-PES. In Figure 7 we show the dissociation probability as a function of the incidence energy for H₂ in its rovibrational ground state ($v = 0$, $J = 0$) and in its rovibrationally excited state ($v = 1$, $J = 1$). We have performed both quasi-classical and quantum calculations. From this figure we can see first that, as already observed for many other molecule–surface systems,[2,3,80–84] the quasi-classical results are in good agreement with the quantum ones. Second, we can see that the agreement between the quantum calculations for the CRP-PW91-PES and the MS-PW91-PES is excellent, proving in this way that the quantum dynamically important regions are similar to the quasi-classical ones for reaction. Similar results have been observed for both gas phase[85,86] and molecule/surface reactions.[42] Interestingly, the agreement between these two PESs is somewhat poorer for the
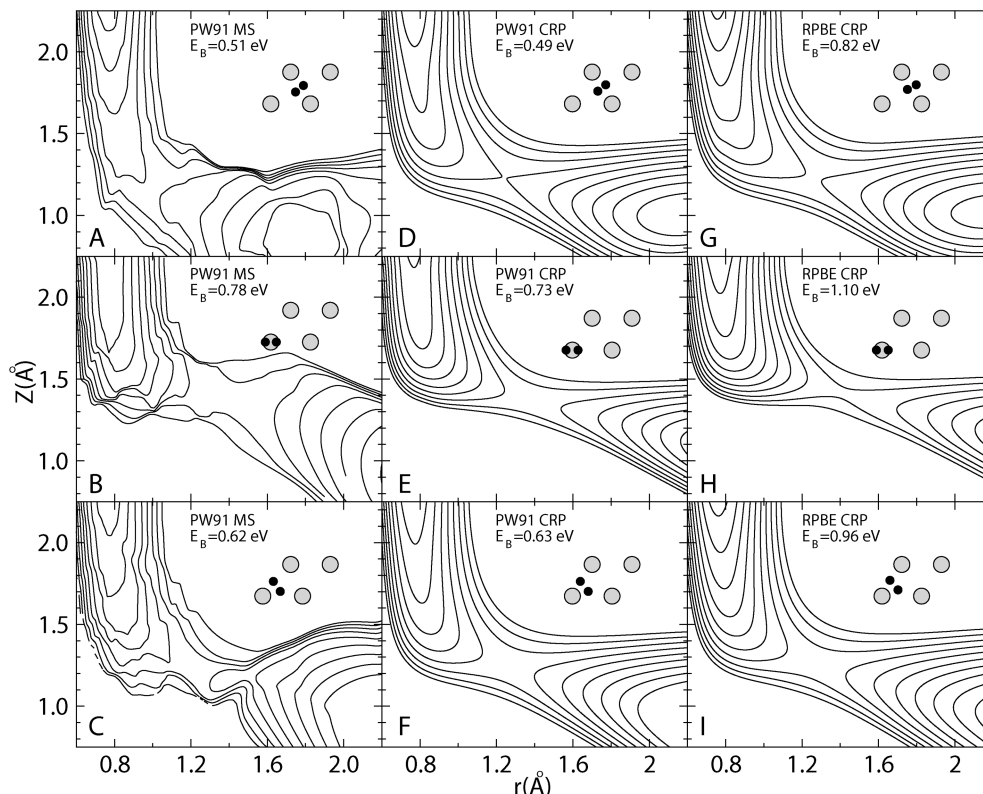
Figure 5. 2D cuts through the MS-PW91-PES (A)−(C), the CRP-PW91-PES (D)−(F), and the CRP-RPBE-PES (G)−(I). (A), (D), (G) Bridge-to-hollow dissociation. (B), (E), (H) Top-to-bridge dissociation. (C), (F), (I) Dissociation above a site halfway between the top and the hcp sites with $\varphi = 120$. The spacing between the contour levels is 0.1 eV.
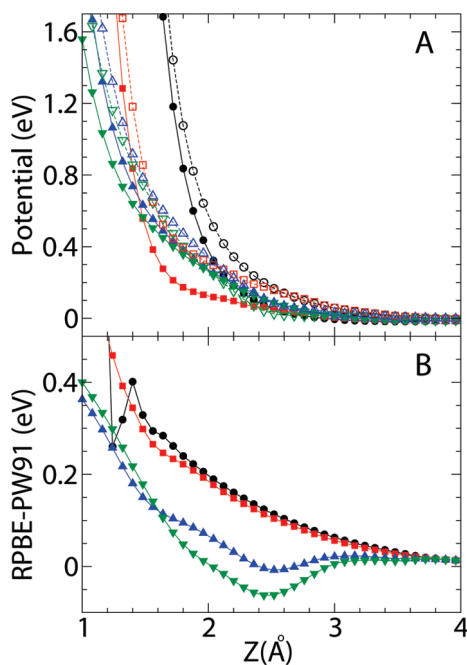

Figure 6. (A) Potential energy as a function of Z: (solid line and solid symbols) PW91 results; (dashed line and open symbols) RPBE results. The configurations displayed are top $\theta = 0$ (black circles); top $\theta = 90$, $\varphi = 0$ (red squares); bridge $\theta = 90$, $\varphi = 0$ (blue triangles pointing up); bridge $\theta = 90$, $\varphi = 40$ (green triangles pointing down). (B) Difference between RPBE and PW91 energies as a function of Z, for the same configurations displayed in the top panel.

quasi-classical calculations. This is so, because quasi-classical calculations are more sensitive to the details of the PES than quantum calculations, where irregular features of the MS-PES may be smoothed out by the delocalization of the wave function.

TABLE 4: Energetic and Geometric Corrugation for the 3 PESs

PES	geometric corr (Å)	energetic corr (eV)
MS-PW91	0.26	0.38
CRP-PW91	0.21	0.39
CRP-RPBE	0.24	0.37

In Figure 7 we have also plotted quasi-classical and quantum dissociation probabilities obtained using the CRP-RPBE-PES. These probabilities are smaller than the ones obtained for the PW91-PESs, which is consistent with the fact that the minimum reaction barriers for these latter PESs are lower than the one for the CRP-RPBE-PES (see Figure 5). But PW91 and RPBE probabilities show the same trends; i.e., if we shift the RPBE (PW91) probabilities down (up) in energy, the curves almost superimpose. A similar dependence of the reactivity on the GGA functional has been found previously for other molecule/surface systems such as N_2/Ru(0001),[44] H_2/Ru(0001),[79] and N_2/W(100) and N_2/W(110).[78]

The good agreement between the MS-PW91-PES and the CRP-PW91-PES simulation obtained for the dissociative adsorption probability should not be surprising because we have used this observable as a convergence criterion for the MS-PES convergence and therefore for stopping the growth process. For this reason we have also tested the accuracy for the scattering probabilities. To perform this analysis, we have only considered quantum dynamics, because quasi-classical dynamics, in general, gives less accurate results when used to analyze events with small probabilities. In Figure 8A we show the final J-summed vibrational excitation probabilities $P(v=0,J=0\rightarrow v=1)$ as a function of the incidence energy. The agreement between the vibrational excitation probability obtained with both PESs, MS-PW91 and CRP-PW91, is almost as good as that for the
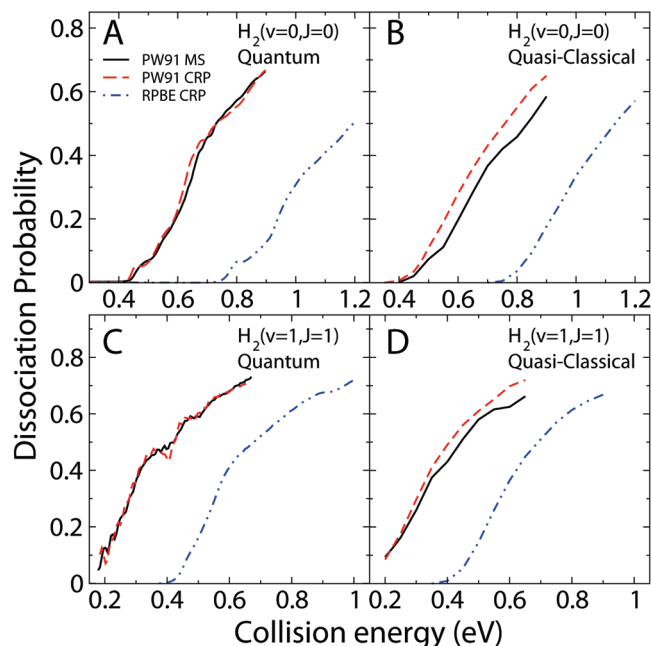
Potential Energy Surfaces for H₂/Cu(111)

J. Phys. Chem. C, Vol. 114, No. 25, 2010 **11199**

Figure 7. Dissociation probability as a function of the incidence energy for CRP-PW91-PES (dashed line), MS-PW91-PES (solid line), and CPR-RPBE-PES (dot-dashed line): (A) H₂ ($v = 0$, $J = 0$) quantum dynamics; (B) H₂ ($v = 0$, $J = 0$) quasi-classical dynamics; (C) H₂ ($v = 1$, $J = 1$) quantum dynamics; (D) H₂ ($v = 1$, $J = 1$) quasi-classical dynamics.

reaction (see Figure 7). If we look at the final m_J-summed rotational excitation probabilities $P(v=0,J=0 \rightarrow v=0,J=2,4)$, plotted in Figure 8B,C, we see that the agreement remains very good, and even for the final m_J-selective transitions $P(v=0,J=0,m_J=0 \rightarrow v=0,J=2,m_J=0,2)$ (see Figure 8D,E) the curves obtained with both PESs are very similar. The comparisons get a little worse for rovibrationally elastic diffraction probabilities, as can be seen in Figure 8F,G, where we have plotted the probabilities for the specular scattering and for first order diffractive scattering (see, for instance, ref 87 for definition of the diffraction order). Nevertheless, the differences between the results obtained with both PESs are small enough to consider the MS interpolation method, interfaced with DFT, suitable to study a wide range of molecule−surface dynamics events, including dissociative adsorption, rotationally elastic scattering, vibrational and rotational excitation, and even diffraction. Similarly good agreement was obtained for H₂/Pt(111), for the MS method interfaced with a previously computed CRP-PES.[42]

We now turn our attention to the comparison of the PW91 and the RPBE dynamics results for scattered molecules (Figure 8), focusing on the PW91 results obtained using the same interpolation method (CRP) as used for RPBE. PW91 and RPBE yield qualitatively similar results for vibrational excitation, which increases with incidence energy until it reaches a maximum, after which it decreases with the collisional energy (Figure 8A). However, the RPBE probabilities are shifted to higher energies with respect to the PW91 ones, the vibrational excitation threshold predicted by the RPBE calculations being higher by about 0.2 eV. For both functionals the actual threshold for vibrational excitation (0.6 and 0.8 eV) is larger than the energetic threshold that would be obtained directly from the vibrational frequency (0.5 eV), which agrees with experimental observation for H₂ + Cu(111).[88] These results are consistent with the presence of higher reaction barriers and slightly weaker curvatures in the RPBE-PES. The curvature of the reaction path determines the coupling between the DOFs responsible for
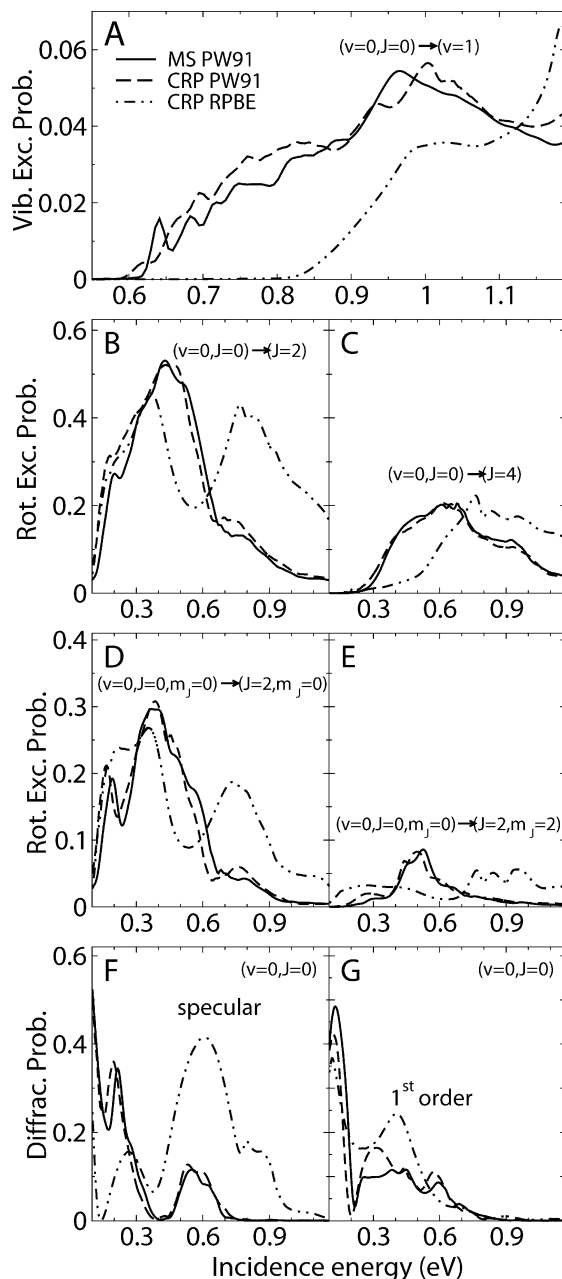

Figure 8. Excitation probabilities calculated with quantum dynamics, as a function of the incidence energy. (A) Vibrational excitation probabilities $P(v=0,J=0 \rightarrow v=1)$. (B) Rotational excitation probabilities $P(v=0,J=0 \rightarrow v=0,J=2)$. (C) Rotational excitation probabilities $P(v=0,J=0 \rightarrow v=0,J=4)$. (D) Rotational excitation probabilities $P(v=0,J=0,m_J=0 \rightarrow v=0,J=2,m_J=0)$. (E) Rotational excitation probabilities $P(v=0,J=0,m_J=0 \rightarrow v=0,J=2,m_J=2)$. (F) Probability of specular diffraction. (G) Probability of first-order diffraction. Key: (solid line) MS-PW91 results; (dashed line) CRP-PW91 results; (dot-dashed line) CRP-RPBE results.

promoting vibrationally inelastic scattering.[89,90] On the other hand, rotational excitation as well as diffraction probabilities, for PW91 and RPBE, present different shapes (see Figure 8B−G). In the case of rotational excitation, both the m_J-summed (Figure 8B,C) and the m_J-selective (Figure 8D,E) excitation probabilities present different shapes as a function of the incidence energy, the ones corresponding to the RPBE-PES being somewhat more structured. Also, important differences can be observed for diffraction (see Figure 8F,G). From Figure 7F,G we can see that the specular scattering probability and the first-order diffraction probability also exhibit different shapes

as a function of incidence energy, the shape depending on the GGA functional used to build the PES. These results show that rotational inelastic scattering and diffraction scattering are quite sensitive to detailed features of the PES.

Conclusion

We have computed three six-dimensional potential energy surfaces (PESs) for H_2/Cu(111) on the basis of accurately interpolated density functional theory (DFT) calculations. To build the PES, we have interpolated a PW91 DFT data set using two different methods, the corrugation reducing procedure (CRP) and the modified Shepard (MS) interpolation method. In applying the CRP method, we have considered two sets of DFT data points obtained by using two GGA/DFT functionals popular in surface science, PW91[55] and RPBE.[56] The three computed PESs have been tested by means of quasi-classical and quantum dynamics.

For the three computed PESs, the MS-PW91-PES, the CRP-PW91-PES, and the CRP-RPBE-PES, we have found that in the minimum reaction barrier geometry, the molecular center of mass is over the bridge site, with the molecule being parallel to the surface. For the CRP-PW91-PES the height of this barrier is 0.49 eV (0.51 eV for the MS-PW91-PES) whereas for the CRP-RPBE-PES it is 0.82 eV. Therefore, the CRP-PW91-PES shows higher reactivity than the CRP-RPBE-PES. The two PESs only show minor differences in corrugation, geometric corrugation differences being less than 0.05 Å and energetic corrugation differences being less than 0.02 eV. Whereas these differences are small enough to ensure that reaction probabilities and vibrational excitation probabilities computed with these PESs exhibit similar shapes as functions of collision energy, the differences are large enough to lead to large changes in rotational excitation and diffractive scattering probability curves. At this point, it is worth mentioning that the only way to distinguish which functional is more suitable is through a comparison with suitable experimental results, with a meaningful comparison requiring a deep knowledge of the experimental details. A detailed comparison between theoretical and experimental results for H_2 (D_2)/Cu(111) has been[52] (and will be[91]) presented elsewhere.

The comparison between the MS results obtained by interfacing the MS method directly with DFT and the CRP results is very good for reaction probabilities and good for scattering probabilities. It is good enough for considering the MS interpolation a good method to obtain PESs for use in studies of reactive molecule−surface scattering. This opens the possibility of polyatomic molecules−surface scattering studies, such as reactive scattering of methane from Ni surfaces, which are presently the subject of an important experimental[92,93] and theoretical[94,95] effort.

References and Notes

(1) Gross, A. *Surf. Sci. Rep.* **1998**, *32*, 291.
(2) Kroes, G. J. *Prog. Surf. Sci.* **1999**, *60*, 1.
(3) Somers, M. F.; Kroes, G. J. *J. Theor. Comput. Chem.* **2005**, *4*, 493.
(4) McCreery, J. H.; Wolken, G. J. *J. Chem. Phys.* **1975**, *63*, 2340.
(5) McCreery, J. H.; Wolken, G. J. *J. Chem. Phys.* **1976**, *64*, 2845.
(6) McCreery, J. H.; Wolken, G. J. *J. Chem. Phys.* **1977**, *67*, 2551.
(7) Dai, J.; Zhang, J. Z. H. *J. Chem. Phys.* **1995**, *102*, 6280.
(8) Persson, M.; Strömquist, J.; Bengtsson, L.; Jackson, B.; Shalashilin, D. V.; Hammer, B. *J. Chem. Phys.* **1999**, *110*, 2240.
(9) Somers, M. F.; Kingma, S. M.; Pijper, E.; Kroes, G. J.; Lemoine, D. *Chem. Phys. Lett.* **2002**, *360*, 390.
(10) Gross, A.; Wilke, S.; Scheffler, M. *Phys. Rev. Lett.* **1995**, *75*, 2718.
(11) Wiesenekker, G.; Kroes, G. J.; Baerends, E. J. *J. Chem. Phys.* **1996**, *104*, 7344.
(12) Martin-Gondre, L.; Crespos, C.; Larregaray, P.; Rayez, J. C.; van Ootergem, B.; Conte, D. *Chem. Phys. Lett.* **2009**, *471*, 136.
(13) Ho, T. S.; Rabitz, H. *J. Chem. Phys.* **1996**, *104*, 2584.
(14) Makarov, D. E.; Metiu, H. *J. Chem. Phys.* **1998**, *108*, 590.
(15) Busnengo, H. F.; Dong, W.; Salin, A. *J. Chem. Phys.* **2000**, *112*, 7641.
(16) Crespos, C.; Collins, M. A.; Pijper, E.; Kroes, G. J. *Chem. Phys. Lett.* **2003**, *376*, 566.
(17) Lorenz, S.; Gross, A.; Scheffler, M. *Chem. Phys. Lett.* **2004**, *395*, 210.
(18) Behler, J.; Delley, B.; Lorenz, S.; Reuter, K.; Scheffler, M. *Phys. Rev. Lett.* **2005**, *94*, 036104.
(19) Ludwig, J.; Vlachos, D. G. *J. Chem. Phys.* **2007**, *127*, 154716.
(20) Busnengo, H. F.; Dong, W.; Salin, A. *Chem. Phys. Lett.* **2000**, *320*, 328.
(21) Busnengo, H. F.; Crespos, C.; Dong, W.; Rayez, J. C.; Salin, A. *J. Chem. Phys.* **2002**, *116*, 9005.
(22) Kresse, G. *Phys. Rev. B* **2000**, *62*, 8295.
(23) di Césare, M. A.; Busnengo, H. F.; Dong, W.; Salin, A. *J. Chem. Phys.* **2003**, *118*, 11226.
(24) Volpilhac, G.; Salin, A. *Surf. Sci.* **2004**, *556*, 129.
(25) Luppi, M.; McCormack, D. A.; Olsen, R. A.; Baerends, E. J. *J. Chem. Phys.* **2005**, *123*, 164702.
(26) Alducin, M.; Díez- Muiño, R.; Busnengo, H. F.; Salin, A. *Phys. Rev. Lett.* **2006**, *97*, 056102.
(27) Busnengo, H. F.; Martínez, A. E. *J. Phys. Chem. C* **2008**, *112*, 5579.
(28) Lozano, A.; Gross, A.; Busnengo, H. F. *Phys. Chem. Chem. Phys.* **2009**, *11*, 5814.
(29) Olsen, R. A.; Busnengo, H. F.; Salin, A.; Somers, M. F.; Kroes, G. J.; Baerends, E. J. *J. Chem. Phys.* **2002**, *116*, 3841.
(30) Riviere, P.; Busnengo, H. F.; Martín, F. *J. Chem. Phys.* **2004**, *121*, 751.
(31) Vincent, J. K.; Olsen, R. A.; Kroes, G. J.; Luppi, M.; Baerends, E. J. *J. Chem. Phys.* **2005**, *122*, 044701.
(32) Salin, A. *J. Chem. Phys.* **2006**, *124*, 104704.
(33) Alducin, M.; Busnengo, H. F.; Díez-Muiño, R. *J. Chem. Phys.* **2008**, *129*, 224702.
(34) Laurent, G.; Martín, F.; Busnengo, H. F. *Phys. Chem. Chem. Phys.* **2009**, *11*, 7303.
(35) Ischtwan, J.; Collins, M. A. *J. Chem. Phys.* **1994**, *100*, 8080.
(36) Collins, M. A. *Theor. Chem. Acc.* **2002**, *108*, 313.
(37) Song, K.; Collins, M. A. *Chem. Phys. Lett.* **2001**, *335*, 481.
(38) Bettens, R. P. A.; Hansen, T. A.; Collins, M. A. *J. Chem. Phys.* **1999**, *111*, 6322.
(39) Fuller, R. O.; Bettens, R. P. A.; Collins, M. A. *J. Chem. Phys.* **2001**, *114*, 10711.
(40) Collins, M. A.; Petrie, S.; Chalk, A. J.; Radom, L. *J. Chem. Phys.* **2000**, *112*, 6625.
(41) Zhang, D. H.; Collins, M. A.; Lee, S. Y. *Science* **2000**, *290*, 961.
(42) Crespos, C.; Collins, M. A.; Pijper, E.; Kroes, G. J. *J. Chem. Phys.* **2004**, *120*, 2392.
(43) van Harrevelt, R.; Honkala, K.; Nørskov, J. K.; Manthe, U. *J. Chem. Phys.* **2005**, *122*, 234702.
(44) Díaz, C.; Vincent, J. K.; Krishnamohan, G. P.; Olsen, R. A.; Kroes, G. J.; Honkala, K.; Nørskov, J. K. *Phys. Rev. Lett.* **2006**, *96*, 096102.
(45) Díaz, C.; Vincent, J. K.; Krishnamohan, G. P.; Olsen, R. A.; Kroes, G. J.; Honkala, K.; Nørskov, J. K. *J. Chem. Phys.* **2006**, *125*, 114706.
(46) Groot, I. M. N.; Juanes-Marcos, J. C.; Díaz, C.; Somers, M. F.; Olsen, R. A.; kroes, G. J. *Phys. Chem. Chem. Phys.* **2010**, *12*, 1331.
(47) Abufager, P. N.; Crepos, C.; Busnengo, H. F. *Phys. Chem. Chem. Phys.* **2007**, *9*, 2258.
(48) Zheng, J.; Zhao, Y.; Truhlar, D. G. *J. Chem. Theory Comput.* **2009**, *5*, 808.
(49) Yang, K.; Zheng, J.; Zhao, Y.; Truhlar, D. G. *J. Chem. Phys.* **2010**, *132*, 164117.
(50) Clary, D. C. *Science* **2008**, *321*, 789.
(51) Mosch, C.; Koukounas, C.; Bacalis, N.; Metropoulos, A.; Gross, A.; Mavridis, A. *J. Phys. Chem. C* **2008**, *112*, 6924.
(52) Janesko, B. G.; Henderson, T. M.; Scuseria, G. E. *Phys. Chem. Chem. Phys.* **2009**, *11*, 443.
(53) Díaz, C.; Pijper, E.; Olsen, R. A.; Busnengo, H. F.; Auerbach, D. J.; Kroes, G. J. *Science* **2009**, *326*, 832.

Potential Energy Surfaces for H$_2$/Cu(111)

J. Phys. Chem. C, Vol. 114, No. 25, 2010 **11201**

(54) Chuang, Y. Y.; Radhakrishnan, M. L.; Fast, P. L.; Cramer, C. J.; Truhlar, D. G. *J. Phys. Chem. A* **1999**, *103*, 4893.

(55) Perdew, J. P.; Chevary, J. A.; Vosko, S. H.; Jackson, K. A.; Pederson, M. R.; Singh, D. J.; Fiolhais, C. *Phys. Rev. B* **1992**, *46*, 6671.

(56) Hammer, B.; Hansen, L. B.; Nørskov, J. K. *Phys. Rev. B* **1999**, *59*, 7413.

(57) Kroes, G. J.; Gross, A.; Baerends, E. J.; Scheffler, M.; McCormack, D. A. *Acc. Chem. Res.* **2002**, *35*, 193.

(58) Nieto, P.; Pijper, E.; Barredo, D.; Laurent, G.; Olsen, R. A.; Baerends, E. J.; Kroes, G. J.; Farías, D. *Science* **2006**, *312*, 86.

(59) http://dcwww.camp.dtu.dk/campos/Dacapo.

(60) Vanderbilt, D. *Phys. Rev. B* **1990**, *41*, 7892.

(61) Thompson, K. C.; Collins, M. A. *J. Chem. Soc., Faraday. Trans.* **1997**, *93*, 871.

(62) Dai, J.; Light, J. C. *J. Chem. Phys.* **1997**, *107*, 1676.

(63) Karplus, M.; Porter, R. N.; Sharma, R. D. *J. Chem. Phys.* **1965**, *43*, 3259.

(64) Stoer, J.; Bulirsch, R. *Introduction to Numerical Analysis*; Springer: New York, 1980.

(65) Swope, W. C.; Andersen, H. C.; Berens, P. H.; Wilson, K. R. *J. Chem. Phys.* **1982**, *76*, 637.

(66) McCormack, D. A.; Kroes, G. J.; Olsen, R. A.; Groeneveld, J. A.; van Stralen, J. N. P.; Baerends, E. J.; Mowrey, R. C. *Faraday Discuss.* **2000**, *117*, 109.

(67) Pijper, E.; Somers, M. F.; Kroes, G. J.; Olsen, R. A.; Baerends, E. J.; Busnengo, H. F.; Salin, A.; Lemoine, D. *Chem. Phys. Lett.* **2001**, *347*, 277.

(68) Riviere, P.; Busnengo, H. F.; Martín, F. *J. Chem. Phys.* **2005**, *123*, 74705.

(69) Kosloff, R. *J. Phys. Chem.* **1988**, *92*, 2087.

(70) Pijper, E.; Kroes, G. J.; Olsen, R. A.; Baerends, E. J. *J. Chem. Phys.* **2002**, *117*, 5885.

(71) Feit, M. D.; Fleck, J. A.; Steiger, A. *J. Comput. Phys.* **1982**, *47*, 412.

(72) Light, J. C.; Hamilton, I. P.; Lill, J. V. *J. Chem. Phys.* **1985**, *82*, 1400.

(73) Kosloff, D.; Kosloff, R. *J. Comput. Phys.* **1983**, *52*, 35.

(74) Corey, G. C.; Lemoine, D. *J. Chem. Phys.* **1992**, *97*, 4115.

(75) Barlint-Kurti, G. G.; Dixon, R. N.; Marston, C. C. *J. Chem. Soc., Faraday Trans.* **1990**, *86*, 1741.

(76) Mowrey, R. C.; Kroes, G. J. *J. Chem. Phys.* **1995**, *103*, 1216.

(77) Neuhauser, D.; Baer, M. *J. Chem. Phys.* **1989**, *91*, 4651.

(78) Bocan, G. A.; Díez-Muiño, R.; Alducin, M.; Busnengo, H. F.; Salin, A. *J. Chem. Phys.* **2008**, *128*, 154704.

(79) Luppi, M.; Olsen, R. A.; Baerends, E. J. *Phys. Chem. Chem. Phys.* **2006**, *8*, 688.

(80) Busnengo, H. F.; Pijper, E.; Somers, M. F.; Kroes, G. J.; Salin, A.; Olsen, R. A.; Lemoine, D.; Dong, W. *Chem. Phys. Lett.* **2002**, *356*, 515.

(81) Busnengo, H. F.; Pijper, E.; Kroes, G. J.; Salin, A. *J. Chem. Phys.* **2003**, *119*, 12553.

(82) Farías, D.; Díaz, C.; Rivière, P.; Busnengo, H. F.; Nieto, P.; Somers, M. F.; Kroes, G. J.; Salin, A.; Martín, F. *Phys. Rev. Lett.* **2004**, *93*, 246104.

(83) Díaz, C.; Somers, M. F.; Kroes, G. J.; Busnengo, H. F.; Salin, A.; Martín, F. *Phys. Rev. B* **2005**, *72*, 035401.

(84) Riviere, P.; Somers, M. F.; Kroes, G. J.; Martín, F. *Phys. Rev. B* **2006**, *73*, 205417.

(85) Collins, M. A.; Zhang, D. H. *J. Chem. Phys.* **1999**, *111*, 9924.

(86) Bettens, R. P. A.; Collins, M. A.; Jordan, M. J. T.; Zhang, D. H. *J. Chem. Phys.* **2000**, *112*, 10162.

(87) Díaz, C.; Busnengo, H. F.; Rivière, P.; Farías, D.; Nieto, P.; Somers, M. F.; Kroes, G. J.; Salin, A.; Martín, F. *J. Chem. Phys.* **2005**, *122*, 154706.

(88) Rettner, C.; Michelsen, H. A.; Auerbach, D. *J. Chem. Phys.* **1993**, *175*, 157.

(89) Darling, G. R.; Holloway, S. *J. Chem. Phys.* **1992**, *97*, 734.

(90) Kroes, G. J.; Wiesenekker, G.; Baerends, E. J.; Mowrey, R. C. *Phys. Rev. B* **1996**, *53*, 10397.

(91) Díaz, C.; Olsen, R. A.; Auerbach, D. J.; Kroes, G. J. *Phys. Chem. Chem. Phys.* **2010**; DOI: 10.1039/c001956a.

(92) Beck, R. D.; Maroni, P.; Papageorgopoulos, D. C.; Dang, T. T.; Schmid, M. P.; Rizzo, T. R. *Science* **2003**, *302*, 98.

(93) Smith, R. R.; Killelea, D. R.; DelSesto, D. F.; Utz, A. L. *Science* **2004**, *304*, 992.

(94) Nave, S.; Jackson, B. *Phys. Rev. Lett.* **2007**, *98*, 173003.

(95) Tiwari, A. K.; Nave, S.; Jackson, B. *Phys. Rev. Lett.* **2009**, *103*, 253201.